Comparison of Results in Flexible Multibody Dynamics Using Various Approaches

OSKAR WALLRAPP

Department of Precision and Micro Engineering, Munich University of Applied Sciences, Lothstr. 34, D-80335 Munich, Germany, e-mail: wallrapp@fhm.edu

SIMON WIEDEMANN

Lenaustrasse 2, D-81373 Munich, Germany, e-mail: simon.wiedemann@web

Abstract. Throughout the past decades a considerable amount of work has been dedicated to the development and application of formalisms to simulate flexible bodies in a multibody system (MBS). The two most common approaches to describe the deformation of a flexible body with respect to their floating frame of reference are to apply the linear finite element formulation and the linear modal approach using global mode shapes.

On the field of flexible body modelling, this paper discusses two topics: a) the consideration of quadratic terms in the equations of deformation and b) the presentation of methods for global mode preparation to reduce the computer time for dynamic simulations without loss of accuracy regarding deformations.

The proposed methods are applied in two examples, for the deformation of a stabilisation linkage of a car's front suspension and for the simulation of the deployment of a flexible solar array.

Keywords: Multibody simulation, flexible body modelling, nodal and modal coordinates, mode selection

1. Introduction

For the simulation and analysis of flexible mechanical systems, the multibody system (MBS) theory is applied. In this methodology, a flexible multibody systems is based on the floating frame of reference formulation with superimposed deformations. Then the flexible body motion is the sum of a large reference motion and small deformations. The displacement field due to deformation is approximated by summing the products of known shape functions and unknown weighing coefficients. The shape functions may be obtained using the finite element approach, where local polynomial functions represent the nodal coordinates or the modal approach, where

global eigenfunctions or static displacement fields represent modal amplitudes. The latter approach reduces the system order but gives rise to the problem of selecting the shape functions. In the following we assume that the strain and displacements are small, but shortening and tilting effects due to high loads should be considered during calculation of the displacement field. The material law is linear.

The multibody system software SIMPACK [4] is based on the formulation above, and the data of flexible bodies are taken from the SID file, and prepared in pre-processors SIMBEAM [10] for spatial beam structures and in FEMBS for general spatial finite element structures in connection with all important commercial finite element software like ANSYS, NASTRAN, etc. The pre-processors generate all mass and stiffness data needed in SIMPACK including geometric stiffness matrices. These prove to be important when buckling or stiffening effects due to large longitudinal loads have to be taken into account [11].

As shown in [10], [3] the linear theory of elasticity is often not accurate enough when structures experience loads that approach the critical loads for buckling and tilting or when spatial bending effects are considered. In such cases a non-linear beam theory or a substructure technique is more suitable. In this paper, kinematic displacement computations are made using also the quadratic terms. The method is implemented in SIMPACK and all required matrices can be pre-calculated in SIMBEAM.

The advantage of the modal approach is the small number of degrees of freedom, thus reducing the computational burden considerably compared to the nodal approach. The modal method however requires the pre-calculation of the mode shapes to be used (for example by solving eigen systems or static problems) in advance of the simulations. As many authors have shown, the quality of results obtained with the modal approach depends (besides numerical aspects) exclusively on the quality of the mode shapes used in the simulations, that is on how accurate the mode shapes can represent the real deformations. Thus since the actual loads, load frequencies and deformations of the bodies are usually not known beforehand, the choice of mode shapes is often random (assumed modes), as are the results of such simulations. It is known that even a very small number of proper mode shapes can lead to results close to or equal to those obtained with a FE approach.

This paper discusses methods for a proper selection of mode shapes in advance of the simulations and compares results using both the nodal and modal approach. Additionally, the

influence of the geometric stiffness matrices and kinematic displacement computation with quadratic terms is studied. The results are compared with results obtained using ANSYS and the nonlinear absolute nodal coordinate formulation (ANCF) [2].

The first example of a stabilisation linkage of a car's front suspension (Figure 1) is a spatial beam structure that is modelled using SIMBEAM. Static and dynamical load cases are simulated using SIMBEAM and SIMPACK. The second example is a flexible satellite solar array (Figure 2). The goal of the simulation is to compute the flexible behaviour during deployment. In addition to [12] new methods for mode shape creation are applied to increase accuracy and to reduce the computational burden. The mode shapes of the flexible bodies (yoke and six panels) are created using NASTRAN and FEMBS and the deployment simulation is made using SIMPACK.

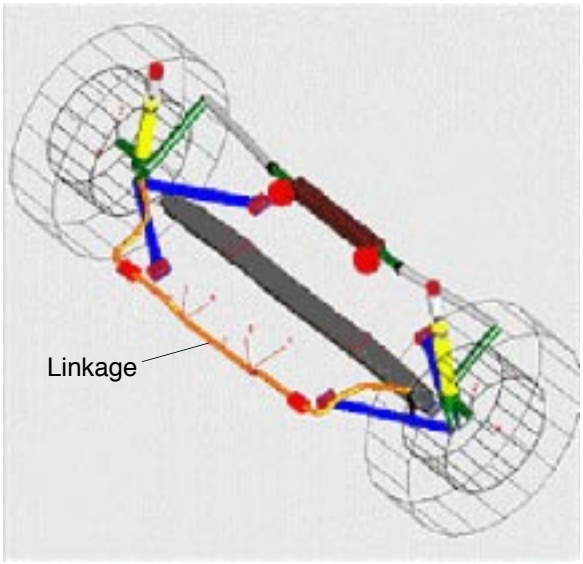

Figure 1. Stabilisation linkage of a car's front suspension.

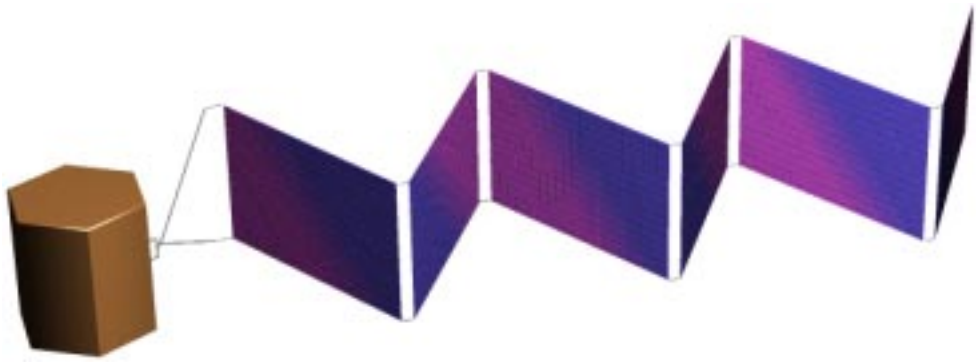

Figure 2. Deployment of a flexible solar array.

2. Basics on Flexible Multibody System Theory

A brief description of the equations of motion of a flexible multibody system as published in many papers [5, 7] is given to explain the notation and to give an overview of the assumptions made for such formulations.

Consider a multibody system of n bodies where the motion is described by a set of position and velocity variables $\mathbf{z}_I^i(t)$ and $\mathbf{z}_{II}^i(t)$, respectively for each body i. A multibody system may now be obtained from the general model of continuum mechanics by formulating three types of constraint equations: (1) definition of the models of bodies (i.e. finite element models, beams, etc.) to be used for a specific analysis; (2) introducing a specific floating frame of reference to describe body deformations; (3) constraints due to joints between the nodes on the bodies. The explicit form of constraints of types 1 and 2 relates the displacement field of all the points of the multibody system to the variables $\mathbf{z}_I^i$ and $\mathbf{z}_{II}^i$, where $\dot{\mathbf{z}}_I^i = \mathbf{Z}^i\ \mathbf{z}_{II}^i$. Holonomic constraints of type 3 due joints $a = 1, .. n_c$, between bodies i and j can be written implicitly as

$$\mathbf{g}^a(\mathbf{z}_I^i, \mathbf{z}_I^j, t) = \mathbf{0} \Leftrightarrow \mathbf{G}^{ai}\ \mathbf{z}_{II}^i + \mathbf{G}^{aj}\ \mathbf{z}_{II}^j + \frac{\partial \mathbf{g}^a}{\partial t} = 0 \ \text{ with } \ \mathbf{G}^{ai} = \frac{\partial \mathbf{g}^a}{\partial \mathbf{z}_I^i}\mathbf{Z}^i,\ \mathbf{G}^{aj} = \frac{\partial \mathbf{g}^a}{\partial \mathbf{z}_I^j}\mathbf{Z}^j. \qquad (1)$$

Formulating all types of constraint equations and applying one of the principles of dynamics, one can generate the system equations in descriptor form or in state space form. An intermediate result of such a derivation of the equations of motion for a system of n flexible bodies is the virtual power expression due to inertia, internal forces of elasticity and applied body and surface forces

$$\delta P = \sum_{i=1}^{n} \boldsymbol{\delta}\mathbf{z}_{II}^{i\,T} \left(-\mathbf{M}^i\ \dot{\mathbf{z}}_{II}^i + \mathbf{h}_\omega^i + \mathbf{h}_e^i + \mathbf{h}_g^i + \mathbf{h}_f^i + \mathbf{h}_c^i \right) = 0. \qquad (2)$$

The matrices $\boldsymbol{\delta}\mathbf{z}_{II}^i$ are the virtual velocities, belonging to the generalized velocities $\mathbf{z}_{II}^i$, $\mathbf{M}^i$ and $\mathbf{h}_c^i$ are the corresponding generalized masses and constraint forces, respectively. $\mathbf{h}_\omega^i$ are generalised inertia forces due to motion of the body reference frame, $\mathbf{h}_e^i$ represents the internal forces due to deformations, and $\mathbf{h}_g^i$ and $\mathbf{h}_f^i$ consider gravitational forces and nodal forces and torques on body i, respectively.

Jourdain's principle states that the virtual power of the constraint forces, result of all types of constraints, is zero. In Equation (2), the virtual power expressions due to constraints of type 1 and 2 do not appear, but the virtual power due to constraints of type 3 is given explicitly. The expression

$$\mathbf{M}^i \, \dot{\mathbf{z}}^i_{II} = \mathbf{h}^i_\omega + \mathbf{h}^i_e + \mathbf{h}^i_g + \mathbf{h}^i_f + \mathbf{h}^i_c \tag{3}$$

together with Equation (1) are the equations of motion of a body *i*, where $\mathbf{h}^i_c$ are the generalised constraint forces due to joints on body *i*.

In this formulation the flexible body motion is separated into a motion of a floating frame of reference and small deformations. The displacement field due to deformation is approximated by summing the products of known shape functions and unknown weighing coefficients, called the elastic coordinates. Hence, the absolute position $\underline{\rho}$ of a point *P* at physical coordinate $\underline{R}$ on body *i* at time *t* is given by the absolute position $\underline{\rho}^i$ of the body reference frame $\{O^i, \underline{\mathbf{e}}^i\}$ with respect to the inertia frame $\{O^I, \underline{\mathbf{e}}^I\}$ and the relative position $\underline{r}(\underline{R})$, see Figure 3. Here and in all the following, vectors are expressed in coordinates of the body reference frame and are indicated by a bold letter, but the time dependence of variables is not always written.

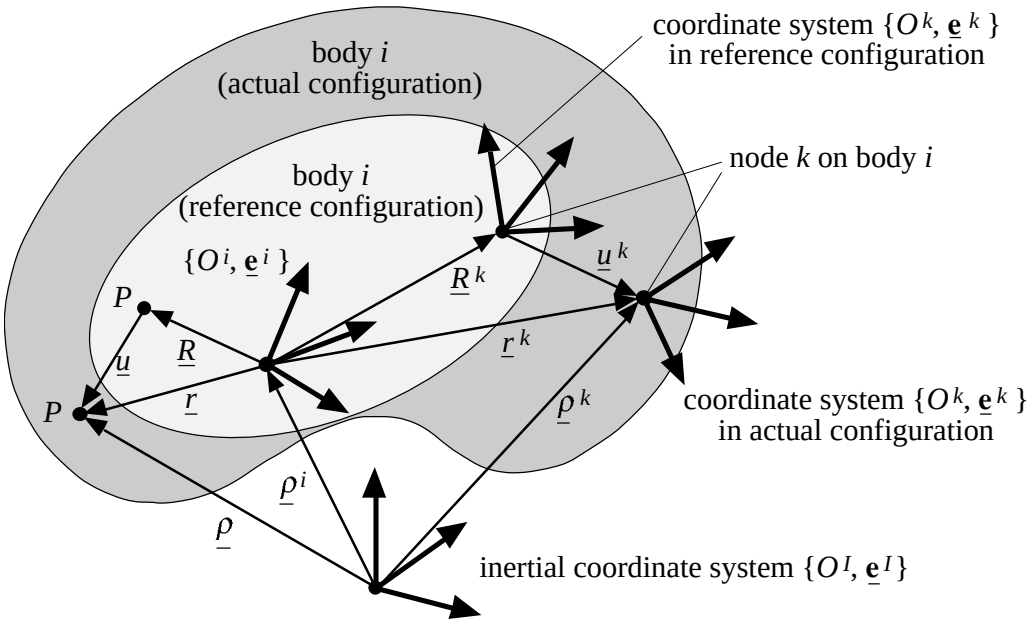

Figure 3 General model of a flexible body i.

The absolute position of P is expressed as

$$\boldsymbol{\rho}(\mathbf{R}) = \boldsymbol{\rho}^i + \mathbf{r}(\mathbf{R}) \quad \text{where} \quad \mathbf{r}(\mathbf{R}) = \mathbf{R} + \mathbf{u}(\mathbf{R}), \tag{4}$$

and where $\mathbf{u}(\mathbf{R}, t)$ is the elastic deflection at $\mathbf{R}$.

The absolute orientation of a coordinate system $\{P, \underline{\mathbf{e}}\}$ attached to a section of a body (in case of beam models attached to the beam section at $\underline{R}_1$) or of a frame $\{O^k, \underline{\mathbf{e}}^k\}$ at a node k on body i (Figure 3) is given by the product of the orientation matrix $\mathbf{A}^i$ of the body reference frame with respect to the inertia frame and the orientation matrix $\boldsymbol{\Theta}(\mathbf{R})$ of the section frame with respect to the body reference frame as

$$\mathbf{A}(\mathbf{R}) = \boldsymbol{\Theta}(\mathbf{R})\, \mathbf{A}^i \quad \text{satisfying} \quad \underline{\mathbf{e}} = \mathbf{A}(\mathbf{R})\, \underline{\mathbf{e}}^I \tag{5}$$

Matrices $\mathbf{A}^i$ and $\boldsymbol{\Theta}$ are parameterised by angles $\boldsymbol{\alpha}^i(t)$ and $\boldsymbol{\vartheta}(\mathbf{R}, t)$, respectively.

Linear velocity $\mathbf{v}$ and angular velocities $\boldsymbol{\omega}$ of a body section at point P are derived by differentiation of Equation (4) with respect to time and using the Poisson formula on Equation (5), thus

$$\begin{aligned}
&\mathbf{v}(\mathbf{R}) = \mathbf{v}^i + \tilde{\boldsymbol{\omega}}^i\, \mathbf{r}(\mathbf{R}) + \dot{\mathbf{r}}(\mathbf{R}) = \mathbf{v}^i - \tilde{\mathbf{r}}(\mathbf{R})\, \boldsymbol{\omega}^i + \dot{\mathbf{r}}(\mathbf{R}) \\
&\boldsymbol{\omega}(\mathbf{R}) = \boldsymbol{\omega}^i + \mathbf{w}(\mathbf{R}) \quad \text{satisfying} \\
&\tilde{\boldsymbol{\omega}}^i \equiv {}^i\tilde{\boldsymbol{\omega}}^{iI} = \mathbf{A}^i\, \dot{\mathbf{A}}^{iT}, \;\; \tilde{\mathbf{w}} \equiv {}^i\tilde{\mathbf{w}}^{ki} = \dot{\boldsymbol{\Theta}}^T \boldsymbol{\Theta}, \\
&\text{where} \quad \dot{\mathbf{r}}(\mathbf{R}) = \dot{\mathbf{u}}(\mathbf{R}) \quad \text{and} \quad \mathbf{w} = \mathbf{W}(\boldsymbol{\vartheta})\, \dot{\boldsymbol{\vartheta}}
\end{aligned} \tag{6}$$

Note that $\mathbf{v}^i$ and $\boldsymbol{\omega}^i$ are the linear and angular velocities of the reference frame. Variables $\boldsymbol{\rho}^i$, $\mathbf{A}^i$, $\mathbf{v}^i$ and $\boldsymbol{\omega}^i$ depend on time t and describe the motion of the reference frame of body i. Variables $\mathbf{r}$, $\boldsymbol{\Theta}$, $\dot{\mathbf{r}}$, and $\mathbf{w}$ or $\mathbf{u}$, $\boldsymbol{\vartheta}$, $\dot{\mathbf{u}}$, and $\dot{\boldsymbol{\vartheta}}$ depend on coordinates $\mathbf{R}$ and time t and represent the deformation of the body. Referring to the specific floating frames of reference such as tangent frame, cord / plane frame, or Tisserand / Buckens frame, $\mathbf{u}$ and $\boldsymbol{\vartheta}$ have to satisfy six constraints of reference conditions given in [7].

The deformation variables in Equations (4) to (6) are approximated by known shape functions $\boldsymbol{\phi}(\mathbf{R})$ and time dependent weighing coefficients or elastic coordinates $\mathbf{q}^i(t)$. In general we can write

$$\mathbf{d}(\mathbf{R},t)=\begin{pmatrix}\mathbf{u}\\ \boldsymbol{\vartheta}\end{pmatrix}=\mathbf{d}\left(\boldsymbol{\phi}(\mathbf{R}),\mathbf{q}^i(t)\right),\quad \dot{\mathbf{d}}(\mathbf{R},t)=\begin{pmatrix}\dot{\mathbf{u}}\\ \dot{\boldsymbol{\vartheta}}\end{pmatrix}=\frac{\partial\mathbf{d}}{\partial\mathbf{q}^i}\,\dot{\mathbf{q}}^i=\boldsymbol{\Phi}(\mathbf{R},\mathbf{q}^i)\,\dot{\mathbf{q}}^i(t) \tag{7}$$

It is assumed that mode shape matrices $\boldsymbol{\phi}(\mathbf{R})$ or $\boldsymbol{\Phi}(\mathbf{R})$ satisfy both the constrains of the chosen continuum model (type 1) and the chosen reference frame (type 2). Thus, the elastic coordinates $\mathbf{q}^i$ are independent of these types of constraints.

Using a linear material law but still a nonlinear strain-displacement relation the virtual power of the internal forces defined in Equation (2) are derived by

$$\delta P_i^i=-\delta\mathbf{z}_{II}^{i\,T}\;\mathbf{h}_e^i=-\int_{V_0^i}\delta\dot{\boldsymbol{\varepsilon}}^T\;\boldsymbol{\sigma}\;dV=-\delta\dot{\mathbf{q}}^{i\,T}\;\mathbf{k}^i, \tag{8}$$

where strain $\boldsymbol{\varepsilon}$, virtual strain velocity $\delta\dot{\boldsymbol{\varepsilon}}$ and stress $\boldsymbol{\sigma}$ are given as

$$\boldsymbol{\varepsilon}(\mathbf{R},t)=\boldsymbol{\varepsilon}(\boldsymbol{\phi},\mathbf{q}^i),\;\delta\dot{\boldsymbol{\varepsilon}}(\mathbf{R})=\mathbf{B}(\mathbf{R},\mathbf{q}^i)\,\delta\dot{\mathbf{q}}^i,\quad \mathbf{B}=\frac{\partial\boldsymbol{\varepsilon}}{\partial\mathbf{q}^i}, \tag{9}$$

$$\boldsymbol{\sigma}(\mathbf{R},t)=\mathbf{H}(\mathbf{R})\,\boldsymbol{\varepsilon}(\mathbf{R},t)+\boldsymbol{\sigma}_0(\mathbf{R}) \tag{10}$$

to give the general internal forces of body i as a nonlinear function of $\mathbf{q}^i$

$$\mathbf{k}^i(\mathbf{q}^i)=\int_{V_0^i}\mathbf{B}^T\;\boldsymbol{\sigma}\;dV=\int_{V_0^i}\mathbf{B}^T(\mathbf{R},\mathbf{q}^i)\left(\mathbf{H}\,\boldsymbol{\varepsilon}(\mathbf{R},\mathbf{q}^i)+\boldsymbol{\sigma}_0\right)dV \tag{11}$$

In Equations (9) to (11), $\mathbf{B}$ is the nonlinear strain matrix, $\mathbf{H}$ is Hooke's matrix, $\boldsymbol{\sigma}_0$ is the matrix of initial stresses and V_0^i is the body volume in the reference configuration.

The equations of motions due to deformations with respect to the reference frame are derived as

$$\mathbf{M}_e^i\,\ddot{\mathbf{q}}^i+\mathbf{D}_e^i\,\dot{\mathbf{q}}^i+\mathbf{k}^i(\mathbf{q}^i)=\sum\int\boldsymbol{\Phi}^T(\mathbf{R},\mathbf{q}^i)\;\;\mathbf{p}^i(\mathbf{R},t) \tag{12}$$

where $\mathbf{M}_e^i$ is the generalized mass matrix, $\mathbf{D}_e^i$ is a matrix of structural damping and $\mathbf{p}^i$ is the matrix of nodal, volume, and inertia forces and torques. $\mathbf{M}_e^i$ is obtained when introducing a matrix of mass properties $\boldsymbol{\pi}$ containing density ρ and inertia moments j_1, j_2, j_3 as

$$\mathbf{M}_e^i = \int_{V_0^i} \mathbf{\Phi}^T \, \boldsymbol{\pi} \, \mathbf{\Phi} \, dV, \quad \boldsymbol{\pi} = diag\left(\rho \;\; \rho \;\; \rho \;\; j_1 \;\; j_2 \;\; j_3\right) \tag{13}$$

All matrices of a flexible body are saved in the SID file where the space dependent integrals are computed in pre-processors such as SIMBEAM or FEMBS together with FE-software, [9].

Finally, the position, velocity and virtual velocity variables of body i introduced in Equations (1) to (3) are given as

$$\mathbf{z}_I^i = \begin{pmatrix} \boldsymbol{\rho}^i \\ \boldsymbol{\alpha}^i \\ \mathbf{q}^i \end{pmatrix}, \qquad \mathbf{z}_{II}^i = \begin{pmatrix} \mathbf{v}^i \\ \boldsymbol{\omega}^i \\ \dot{\mathbf{q}}^i \end{pmatrix}, \qquad \delta\mathbf{z}_{II}^i = \begin{pmatrix} \delta\mathbf{v}^i \\ \delta\boldsymbol{\omega}^i \\ \delta\dot{\mathbf{q}}^i \end{pmatrix} \tag{14}$$

containing the variables of the reference motion and the elastic coordinates of deformation. All other matrices are given in [5, 7]

2. Approximation Models for Deformation Field

Ever since multibody programs have come into existence, various models to approximate the displacement field due to deformations have been discussed, see e.g. [8]. In this report six models are discussed that are briefly described as follows:

(A) Finite element discretisation where the deformation is linearly approximated by an interpolation matrix, nodal coordinates and linear strain and stress relations.

(B) Extension of model (A) by consideration of initial stresses and their linear terms in the nodal coordinates, the so-called geometric stiffness matrix.

(C) Finite element discretisation where the deformation is quadratically approximated by the interpolation matrix, nodal coordinates, linear strain and stress relations and initial stresses.

(D) Reduction of the computational burden in MBS dynamical simulations using the modal approach. Model (C) is reduced to a matrix of mode shapes taken from an eigenvalue or a static analysis.

(E) In addition to eigenmodes frequency response modes [1] are prepared for the mode shape matrix as explained in (D).

(F) The mode shapes taken from models (D) and (E) are selected using participation factors [12].

For comparison of these models, results are partly taken from a nonlinear finite element theory – here the absolute nodal coordinate formulation (ANCF) [2] and ANSYS. The six models are described in detail next.

2.1 Model (A) – Linear FE Formulation

The simplest model is a linear expression of the deformation field in Equation (7). Thus, the deformation field of an element *e* at all local element points $\mathbf{x}$ is described by the interpolation matrix $\mathbf{N}^e(\mathbf{x})$ and nodal element coordinates $\mathbf{z}^e(t)$. One finds the following relations for the deformation, strain $\boldsymbol{\varepsilon}$ and stress $\boldsymbol{\sigma}$ of element *e* (denoted by the superscript *e*)

$$\mathbf{d}^e(\mathbf{R},t) = \mathbf{N}^e(\mathbf{x})\,\mathbf{z}^e(t), \qquad \dot{\mathbf{d}}^e(\mathbf{R},t) = \mathbf{N}^e(\mathbf{x})\,\dot{\mathbf{z}}^e(t) \quad \text{and} \tag{15}$$

$$\boldsymbol{\varepsilon}^e(\mathbf{x},t) = \mathbf{B}_L^e(\mathbf{x})\,\mathbf{z}^e(t), \qquad \delta\dot{\boldsymbol{\varepsilon}} = \mathbf{B}_L^e\,\delta\dot{\mathbf{z}}^e, \qquad \boldsymbol{\sigma}^e(\mathbf{x},t) = \mathbf{H}^e(\mathbf{x})\,\boldsymbol{\varepsilon}^e(\mathbf{x},t), \tag{16}$$

where $\mathbf{x} = \mathbf{R} - \mathbf{R}^e$ and $\mathbf{R}^e$ is the position vector of the local element frame, $\mathbf{B}_L^e$ is the linear strain and $\mathbf{H}^e$ the linear Hooke matrix of an element *e*.

The motion of all elements can be written by all global nodes forming the nodal coordinate vector $\mathbf{z}_F$ of the unsupported finite element (FE) structure. Finally, a nodal state vector $\mathbf{y}_F$ of the supported structure embedded into the MBS floating frame of reference is introduced, satifsying both,

$$\mathbf{z}^e = \mathbf{T}^e\,\mathbf{z}_F \quad \text{and} \quad \mathbf{z}_F = \mathbf{J}_F\,\mathbf{y}_F + \bar{\mathbf{J}}_F\,\bar{\mathbf{z}}_F, \tag{17}$$

where $\mathbf{T}^e$ ist a transformation matrix and $\mathbf{J}_F$ and $\bar{\mathbf{J}}_F$ are projection matrices for the free and locked motions of the FE-boundaries. In Equation (17) the supported node motion $\bar{\mathbf{z}}_F$ is mostly zero. This leads with the identy $\mathbf{q}^i \equiv \mathbf{y}_F$ and Equation (15) in accordance to (7)

$$\mathbf{d} = \boldsymbol{\Phi}\,\mathbf{q}^i \qquad \text{where} \qquad \boldsymbol{\Phi}(\mathbf{R}) \equiv \boldsymbol{\Phi}_L = \mathbf{N}^e(\mathbf{x})\,\mathbf{T}^e\,\mathbf{J}_F. \tag{18}$$

$\boldsymbol{\Phi}_L$ is the linear mode shape matrix. From Equations (15) and (16) one derives the internal forces and the mass matrix as given in Equations (11) to (13)

$$\mathbf{k}^i(\mathbf{q}^i) = \mathbf{K}^i_e\, \mathbf{q}^i, \quad \mathbf{K}^i_e = \mathbf{J}_F^T \sum_e \left(\mathbf{T}^{eT}\, \mathbf{K}^e\, \mathbf{T}^e \right) \mathbf{J}_F\,, \quad \mathbf{K}^e = \int\limits_{V_0^e} \mathbf{B}_L^{eT}\, \mathbf{H}^e\, \mathbf{B}_L^e\, dV^e \tag{19}$$

$$\mathbf{M}^i_e = \mathbf{J}_F^T \sum_e \left(\mathbf{T}^{eT}\, \mathbf{M}^e\, \mathbf{T}^e \right) \mathbf{J}_F\,, \quad \mathbf{M}^e = \int\limits_{V_0^e} \mathbf{N}^{eT}\, \boldsymbol{\pi}^e\, \mathbf{N}^e\, dV^e \tag{20}$$

$\mathbf{K}^e$ and $\mathbf{M}^e$ respectively are the element stiffness and mass matrices.

For various models of finite elements, interpolation matrices and their stiffness and mass matrices are given in standard FE books. Model (A) is only useful for small elastic deformations. The loads should be small compared to critical loads, for example for buckling and tilting.

2.2 Model (B) – Geometric Stiffness Matrix

Model (A) is extended by initial stresses $\boldsymbol{\sigma}_0$ as shown in Equation (10) and a bilinear term in the virtual strain velocity, Equation (9). This bilinear term may be derived by a geometrically nonlinear theory, for example for beam [5] and plate models. With the interpolation matrix given for model (A), one finds instead of Equations (16) and (19)

$$\boldsymbol{\varepsilon}^e = \mathbf{B}_L^e\, \mathbf{z}^e, \quad \delta\dot{\varepsilon}_\alpha = \left(\mathbf{B}^e_{L\alpha} + \mathbf{z}^{eT}\, \mathbf{B}^e_{Q\alpha} \right) \delta\dot{\mathbf{z}}^e, \quad \boldsymbol{\sigma}^e = \mathbf{H}^e\, \boldsymbol{\varepsilon}^e + \boldsymbol{\sigma}^e_o \tag{21}$$

$$\mathbf{k}^i(\mathbf{q}^i) = \left(\mathbf{K}^i_e + \mathbf{K}^i_{\text{geo}} \right) \mathbf{q}^i, \quad \mathbf{K}^i_{\text{geo}} = \mathbf{J}_F^T \sum_e \left(\mathbf{T}^{eT}\, \mathbf{K}^e_{\text{geo}}\, \mathbf{T}^e \right) \mathbf{J}_F\,. \tag{22}$$

In Equation (21) subscript α depends on the strain variables of a FE model. Matrix $\mathbf{K}^i_{\text{geo}}$ is the geometric stiffness matrix. The element matrix $\mathbf{K}^e_{\text{geo}}$ leads to the specific initial element stresses $\boldsymbol{\sigma}^e_o$ that are caused by initial loads on FE structures.

Applying the linear theory of elasticity, the actual geometric stiffness matrix of an element can be expressed as a superposition of single load cases L_j on body i and unit geometric stiffness matrices $\widehat{\mathbf{K}}^e_{\text{geo j}}$ that are pre-calculated for unit loads. This gives unit stresses $\boldsymbol{\sigma}^e_{oj}$, see e.g. [11],

$$\mathbf{K}^e_{\text{geo}} = \sum_j \widehat{\mathbf{K}}^e_{\text{geo}\,j}\, L_j\,, \quad \widehat{\mathbf{K}}^e_{\text{geo}\,j} = \sum_\alpha \int\limits_{V_0^e} \mathbf{B}^{eT}_{Q\alpha}\, \sigma^e_{0\alpha\, j}\, dV^e \tag{23}$$

For the deformations and the mass matrix, Equations (18) and (20) are still applied.

Model (B) allows to calculate the critical buckling and tilting load for beam structures and to take other stiffening effects into account, for example on rotating structures. On the other hand, it should be noted that the model does not compute nonlinear displacements such as the shortening of a beam when bent.

2.3 Model (C) – Quadratic Formulation of Deformations

Applying nonlinear theory, for example for a beam element, the Cartesian deformation variables **d** contain quadratic terms and are expressed by integrals of the beam deformations such as longitudinal strain ε and the three curvatures κ_α. The strain relation (21) is still valid, but for **d** = (d_α) instead of Equations (15) and (18) one writes with the linear shape function matrix $\mathbf{N}_L^e = \left(\mathbf{N}_{L\alpha}^e\right)$ and a 6×6 quadratic expansion shape function matrix $\mathbf{N}_{Q\alpha}^e$, for direction α,

$$\begin{aligned} d_\alpha(\mathbf{x}) &= \mathbf{N}_{L\alpha}^e(\mathbf{x})\,\mathbf{z}^e + \tfrac{1}{2}\mathbf{z}^{eT}\,\mathbf{N}_{Q\alpha}^e(\mathbf{x})\,\mathbf{z}^e \quad \text{and} \\ d_\alpha(\mathbf{R}) &= \mathbf{\Phi}_{L\alpha}(\mathbf{R})\,\mathbf{q}^i + \tfrac{1}{2}\mathbf{q}^{iT}\,\mathbf{\Phi}_{Q\alpha}(\mathbf{R})\,\mathbf{q}^i\,, \quad \alpha = 1,\ldots 6 \end{aligned} \tag{24}$$

Note that $\mathbf{\Phi}_{Q\alpha}$ is a $n_q \times n_q$ matrix given as

$$\mathbf{\Phi}_{Q\alpha}(\mathbf{R}) = \overline{\mathbf{T}}^T \sum_e \left(\mathbf{T}^{eT}\,\mathbf{N}_{Q\alpha}^e(\mathbf{x})\,\mathbf{T}^e\right)\overline{\mathbf{T}}\,. \tag{25}$$

If the longitudinal stress and the bending moment of a beam element is constant with respect to the central axis *x*, then matrices $\mathbf{N}_{Q\alpha}^e$ at node *k* are equivalent to the negative values of the unit geometric stiffness matrices $\hat{\mathbf{K}}_{\mathrm{geo}\,j}^e$, where *j* denotes the load case at node *k* in direction α. More details are given in [10].

Model (C) gives better results than models (A) and (B) if the actual loads approach the critical loads for buckling or tilting or if three dimensional bending and torsion motions of beam elements are analysed.

2.4 Model (D) – Modal Transformation

The modal approximation is applied. The deformation of the FE structure of a body *i* is given by Equation (12) where damping is neglected and internal forces are incorporated by a simple stiffness matrix as given in Equation (19). This leads the equations of motion of a FE-structure

$$\mathbf{M}_e^i\ \ddot{\mathbf{y}}_F + \mathbf{K}_e^i\ \mathbf{y}_F = \sum \int \mathbf{\Phi}_L^T\ \mathbf{p}^i\,, \tag{26}$$

where $\mathbf{y}_F$ is the vector of nodal coordinates of the supported FE structure. The length n_{yF} of $\mathbf{y}_F$ is in general very large.

With Equation (26) eigenvectors and static displacement fields due to specific load cases (static modes) can be created to give a small number (n_q) of mode shapes that are taken into account in the dynamic MBS simulation. The selected mode shapes form the mode matrix $\mathbf{S}_e$ with dimensions n_{yF} times n_q. This yields the new mass, stiffness (modal) and mode shape matrices as

$$\begin{aligned} &\mathbf{y}_F = \mathbf{S}_e\ \mathbf{q}^i \quad \text{and} \\ &\mathbf{M}_e^i := \mathbf{S}_e^T\ \mathbf{M}_e^i\ \mathbf{S}_e\,, \quad \mathbf{K}_e^i := \mathbf{S}_e^T\ \mathbf{K}_e^i\ \mathbf{S}_e\,, \quad \mathbf{\Phi} := \mathbf{\Phi}\ \mathbf{S}_e \end{aligned} \tag{27}$$

respectively, with the reduced dimension n_q to approximately describe the deformation of the flexible body as shown in Equation (12). It should be noted that for model (B) also the geometric stiffness matrix $\mathbf{K}^i_{\text{geo}}$ and for model (C) the quadratic mode shape matrices $\mathbf{\Phi}_{Q\alpha}$ have to be transformed to modal form. If all modes shapes are orthogonal the modal mass matrix can be scaled to give an identity matrix.

In general, the lower eigenmodes are more important than the higher frequency modes, and static modes increase the accuracy of the modal approximation, see e. g. [6, 7].

2.5 Model (E) – Using Frequency Response Modes

In addition to eigenmodes the author of [1] proposes a set of frequency response modes that can be computed if harmonic loads $\mathbf{p}_k$ with a main excitation frequency Ω_0 at nodes k can be estimated. With the approximation $\ddot{\mathbf{q}}_F = -\Omega_0^2\ \mathbf{q}_F$, Equation (26) gives

$$\left(-\mathbf{M}_e^i\ \Omega_0^2 + \mathbf{K}_e^i\right) \mathbf{y}_{Fk}^* = \mathbf{\Phi}_L^T\ \mathbf{p}_k \tag{28}$$

and the solution is a displacement field $\mathbf{y}_{Fk}^*$, the so-called frequency response mode. Eigenmodes and frequency response modes form the mode matrix $\mathbf{S}_e$ with dimensions n_{yF} times n_q. The modal transformation is done as described for model (D).

2.6 Mode Selection Using Participation Factors

As proposed in [12], accounting for the joints and loads acting on a flexible body during MBS simulations the selection of mode shapes can be done using pre-calculated participation factors. First a large number of mode shapes and the corresponding modal equations as shown in model (D) are created. Second, loads such as nodal and inertial forces or torques are assumed or estimated. Third, a simple static analysis of this system gives deformations at interesting points of the body that are weighted with the used mode shapes to give the (participation) factors. Scaled factors smaller than a desired value indicate that the share of the corresponding mode shape in the overall deformation is less than this value and may be neglected. The remaining modes are taken into account for time simulations.

It is noted that the participation factors are computed for only one situation or point in time and have to be computed for each individual force and joint configuration. However, when using the method to save computer time the factors would be computed for the most interesting force and joint configurations to give good results for these critical points in time.

The approach is based on the assumption that modes shapes and modal mass and stiffness matrices are prepared for a corresponding floating frame of reference (e.g. a Buckens frame or a tangent frame) and the deformations have no significant backward influence on the body reference motion. Therefore, dominant applied and constraint forces and torques due to force elements, joints, external surface and body loads can be taken from a "simple and quick" rigid body simulation. The equations of motion with respect to the body reference frame (the equations of deformation) are expressed by the coordinates $\mathbf{q}^i$ and $\dot{\mathbf{q}}^i$, the third row of $\mathbf{z}_I^i$ and $\mathbf{z}_{II}^i$ in Equations (14). Thus, from Equation (3) one extract the equations of deformation, when neglecting Coriolis and damping terms, (for more details see [5, 7]),

$$\mathbf{C}_t^i\,\dot{\mathbf{v}}^i + \mathbf{C}_r^i\,\dot{\boldsymbol{\omega}}^i + \mathbf{M}_e^i\,\ddot{\mathbf{q}}^i + \mathbf{K}_e^i\,\mathbf{q}^i = -\mathbf{C}_t^i\left(\tilde{\boldsymbol{\omega}}^i\,\mathbf{v}^i - \mathbf{g}^i\right) - \mathbf{O}_{e0}^i\,\boldsymbol{\omega}_q^i + \sum_k \boldsymbol{\Phi}^{ki\,T}\begin{pmatrix}\mathbf{F}^{ki}\\ \mathbf{L}^{ki}\end{pmatrix} \tag{28}$$

Here $\mathbf{v}^i$, $\boldsymbol{\omega}^i$ are the linear and angular velocity of the reference frame, $\boldsymbol{\omega}_q^i$ contains the quadratic terms of $\boldsymbol{\omega}^i$, $\mathbf{C}_t^i$, $\mathbf{C}_r^i$, and $\mathbf{O}_{e0}^i$ are corresponding mass coefficient matrices, $\mathbf{F}^{ki}$ and $\mathbf{L}^{ki}$ are nodal forces and torques at node *k* including applied and constraint forces, and $\boldsymbol{\Phi}^{ki}$ is the mode shape matrix for node *k*.

Since the constraint forces at joints on the body are conform with the applied forces upon the body, Equation (28) describes the deformations of the body with respect to the constrained floating frame of reference. With the assumption $\ddot{\mathbf{q}}^i = -\Omega_0^2\,\mathbf{q}^i$, where Ω_0 is an assumed excitation frequency to consider inertia forces, from Equation (28) the following LAEs for the elastic coordinates $\mathbf{q}^i$ are solved

$$\left(\mathbf{K}_e^i - \Omega_0^2\,\mathbf{M}_e^i\right)\mathbf{q}^i = \mathbf{h}_{e*}^i \qquad \text{with}$$

$$\mathbf{h}_{e*}^i = \underbrace{-\mathbf{C}_t^i\left(\dot{\mathbf{v}}^i + \tilde{\boldsymbol{\omega}}^i\,\mathbf{v}^i - \mathbf{g}^i\right) - \mathbf{C}_{r0}^i\,\dot{\boldsymbol{\omega}}^i - \mathbf{O}_{e0}^i\,\boldsymbol{\omega}_q^i}_{\text{known inertia forces}} + \underbrace{\sum_k \boldsymbol{\Phi}^{ki\,T}\begin{pmatrix}\mathbf{F}^{ki}\\ \mathbf{L}^{ki}\end{pmatrix}}_{\text{known nodal forces}} \tag{29}$$

From the solution of Equation (29) the deformation of the body can be linearized and calculated using Equations (7) and (18). Thus, the three translational and three rotational deformations of a nodal frame at node *k* on body *i* are

$$\mathbf{d}^{ki} = \left[d_\alpha^{ki}\right], \qquad d_\alpha^{ki} = \sum_{l=1}^{n_q^i} d_{\alpha l}^{ki}\,, \qquad d_{\alpha l}^{ki} = \Phi_{\alpha l}^{ki}\,q_l^i\,, \qquad \alpha = 1,\ldots,6\,. \tag{30}$$

The modal participation factors (MPF) of translational and rotational deformations are defined as

$$P_{\alpha l} = \frac{\left|d_{\alpha l}^{ki}\right|}{\sum_{l=1}^{n_q^i}\left|d_{\alpha l}^{ki}\right|} = \frac{\left|\Phi_{\alpha l}^{ki}\,q_l^i\right|}{\sum_{l=1}^{n_q^i}\left|\Phi_{\alpha l}^{ki}\,q_l^i\right|} < 1 \tag{31}$$

and represent the contribution of mode *l* to the total elastic motion of node *k* along or about α. Since all modes are orthogonalized and thus have no mutual coupling, the coordinates $\mathbf{q}^i$ computed before can be used again together with the $\boldsymbol{\Phi}^{ki}$ to give an estimate of the errors when using a selection of mode shapes compared with the results when using all modes. These errors e_α can be computed for all six degrees of elastic freedom α of node *k* using

$$e_{\alpha k} = \sum_{l=1}^{n_{q,all}^i}\left|\Phi_{\alpha l}^{ki}\,q_l^i\right| - \sum_{l=1}^{n_{q,sel}^i}\left|\Phi_{\alpha l}^{ki}\,q_l^i\right|, \tag{32}$$

where $n^i_{q,all}$ indicate the set of all modes and $n^i_{q,sel}$ the set of selected modes. It is noted that using Equation (32), the errors are absolute and in the correct physical units of either meters or rad.

3. Simulations of a Stabilisation Linkage

The models for the approximation of the deformation field of a flexible body within a MBS are tested first on a stabilisation linkage of a car front suspension, see Figure 1. The spatial curved linkage as shown in Figure 4 is modelled by a 3D beam mesh using 20 nodes for the physical points and an additional node k = 21 for the body reference frame. The mesh has 19 beam elements, thus the mesh leads to a polygon curve of the beam's central line. The number of DOF's of the unsupported structure is n_F = 120, the number of DOF's of the constrained linkage is n^i_q = 114. The cross section area of linkage is like a circle with diameter 0.019 m, the material is steel.

In Figure 5 the first eigenmode of the unsupported linkage is plotted, using the Buckens frame of reference. The values of the first ten eigenfrequencies are 45.0, 96.7, 113.0, 118.2, 202.4, 286.1, 335.9, 367.9, 430.5 and 521.6 Hz. To discuss the described approximations for deformations, the linkage is constrained at various nodes and loaded by a spatial force **F** and torque **L** at node 20, thus $\mathbf{p}^{20} = (F_x\ F_y\ F_z\ L_x\ L_y\ L_z)^T$. The specific load cases are listed in Table 1.

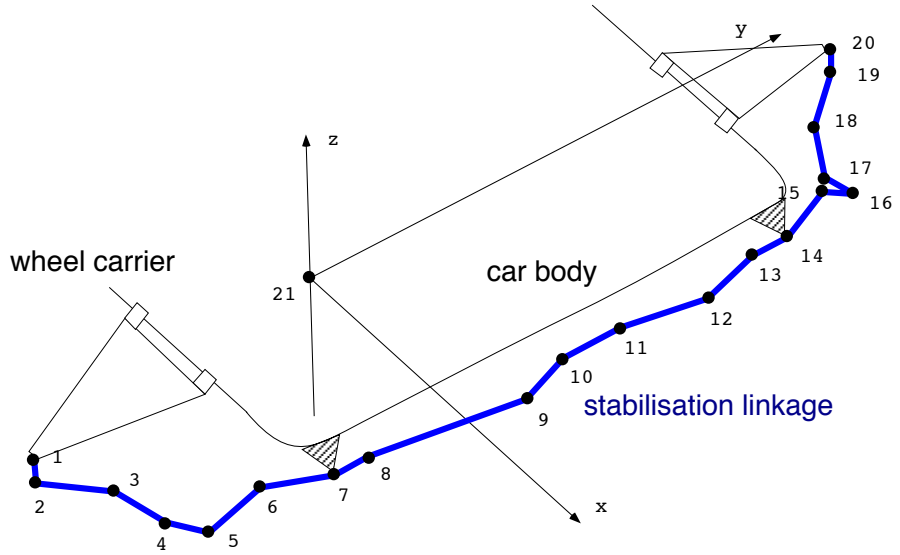

Figure 4. FE-mesh of the stabilisation linkage.

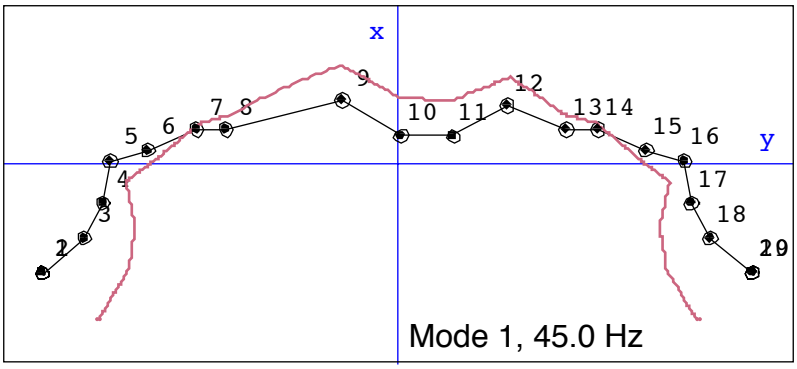

Figure 5. First eigenmode of the unsupported linkage.

Linear vs. quadratic approximation

To discuss the effects of a quadratic approximation field of the deformation, the linkage is analysed for load cases 1, 2 and 3. For load case 3 the deformed and undeformed linkage are plotted in Figure 6. Table 2 lists the results of the displacements at node 20, $\mathbf{d}^{20} = (u_x\ u_y\ u_z\ \vartheta_x\ \vartheta_y\ \vartheta_z)^T$. Here the results obtained with the ANCF method serves as the reference solution with 360 DOF's. For comparison, nonlinear ANSYS results of a model with 600 DOF's are also given in Table 2.

For the three load cases, the error of the linear model (A) for the displacement u_y is very large. With a growing force (compare case 1 and case 2) also other displacements show errors larger than 3 %. Model (C) dramatically reduces the errors for load case 2 from 33 % to 3.5 %. This implies that the quadratic approximation of the deformation field is a powerful model to describe deformations far beyond the linear case. However, for load case 3 the linkage is largely deformed due to the quadratic formulation, see Fig 6.

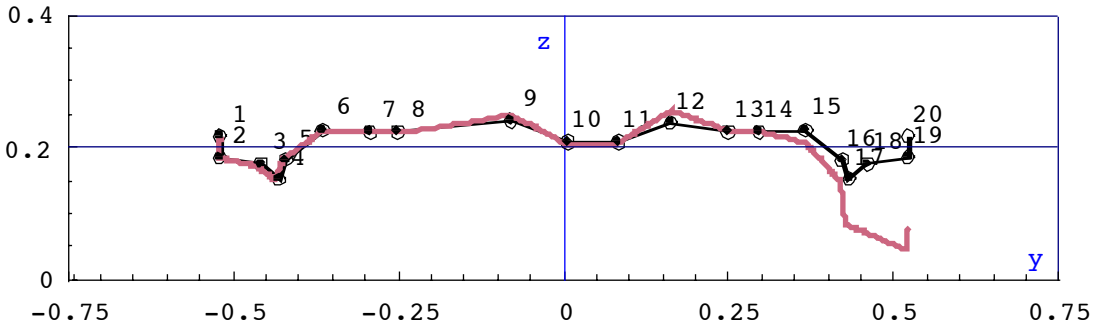

Figure 6. Deformation of the linkage for load case 3.

Nodal vs. modal approximation and mode selection

In the following simulations the modal approximation with a model reduction is applied. With the modelling options in SIMBEAM and SIMPACK, eigenmodes of the unsupported linkage with a Buckens frame of reference are prepared. It should be noted that for the modal formulation the linkage suspension (six constraints) has to satisfy Equation (1). The six coordinates of the reference frame must be included in the equations of motion, Equation (3),, together with six Lagrange multipliers representing the constraints. The number of DOF's is thus n_q + 12. For all models a linear theory of deformation is applied, but body reference motions are computed nonlinearly in SIMPACK.

Besides a simple truncation of higher eigenmodes, a mode selection using participation factors as described in section 2.6 is applied. For load case 2 a graph of factors is plotted in Figure 7. In the fist case, these19 eigenmodes are selected: 1 to 10, 12 to 16, 18, 26, 26, and 27. For load case 3 and 4 with other constraints, a new set of eigenmodes is prepared using participation factors: 14 eigenmodes with the numbers 1 to 6, 8, 9, 11, 12, 14, 16, 26, and 27 are used.

To increase the accuracy of the results, two sets of frequency response modes for an excitation frequency of Ω_0 = 20 Hz with forces at nodes 1 and 20 for load case 2 and at nodes 1, 7, 14 and 20 for load cases 3 and 4 are prepared using Equation (27), in addition to a few number of eigenmodes. The simulation results are listed in Table 3. To test the mode selection for dynamical models, a harmonic load function (load case 4) is applied. Figure 8 shows the computed displacements u_y and u_z (t).

Since the linkage is a 3-dimensional structure, all bending and torsion modes are excited by loads at node 20. Thus only a wide range of eigenmodes can describe the deformation of the body correctly, as shown by the participation factors in Figure 7. It is seen that modes 11 and 17 are not important for the load case 2, whereas modes 26 and 27 are. From Equation (32), an error of -10 % is estimated for displacement u_x at node 20. This value is near by -11 % found by SIMPACK, see Table 3, laod case 2, model approximation 19 em-pf.

A mode selection using participation factors for load case 2 reduces the error from 46 % to 20 % at maximum with respect to the nonlinear results. This mode set needs 100 times less CPU time for load case 4 than the full model with 114 modes while the displacements are

similar, see Figure 8. A set with 9 modes allows for main deformations but cannot correctly represent *y*-motion. Table 3 and Figure 8 also show that even using only 3 eigen-modes together with 12 frequency response gives results in close agreement to the reference of the full model. The reason is that the frequency response modes are a mixture of both static and dynamic modes and account for correct boundary conditions.

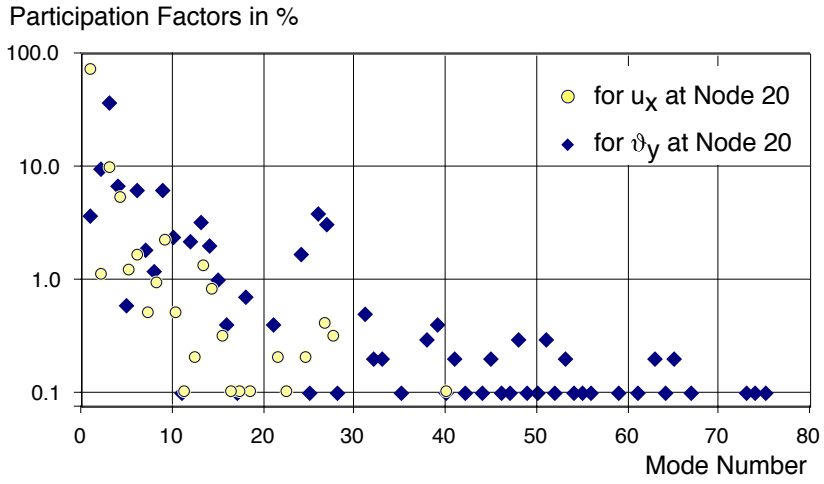

Figure 7. Participation factors of the linkage for load case 2.

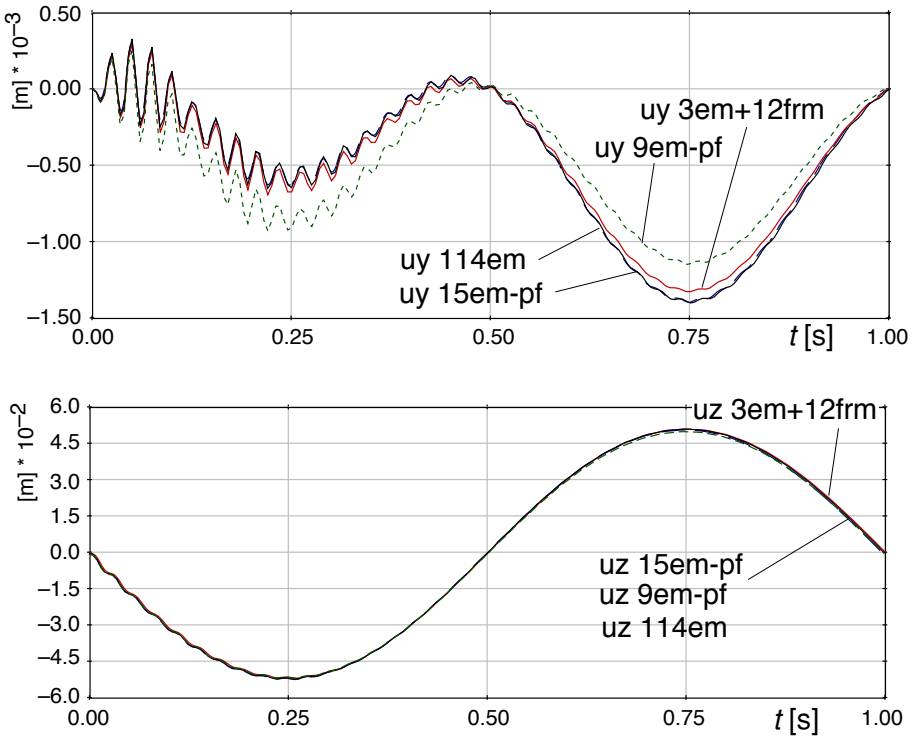

Figure 8. Displacements u_x and u_z of the linkage at node 20 for load case 4.
em = eigenmodes, pf = selected using participation factors, frm = frequency response modes.

4. Simulation of the Deployment of a Solar Array

Due to the complexity of this model as shown in Figure 2 and the fact that about 500 real time seconds must be covered, time simulations using nodal coordinates to serve as a reference for the true deformations or their best approximations cannot be made in a sensible amount of time. Consequently only a modal representation of the deformation of the flexible bodies can be applied.

In reality the deployment of the solar array basically takes place in three steps, see Figure 9 and [12]. In the first step some fixations are released and the deployment springs with a constant torque start working on the yoke and panels, trying to move them. However, since all panels and the yoke are connected via flexible closed cable loops and since the yoke cannot move due to a motor gear unit not activated yet, the springs drive the bodies versus the cables, starting a damped oscillation. This is called jump-out. The second step is the activation of the motor gear unit after 250 seconds, which slowly and smoothly turns the yoke and thus all connected panels. The last step is the final deactivation of the motor gear unit and the activation of lock mechanisms when the array is completely deployed after about 360 seconds.

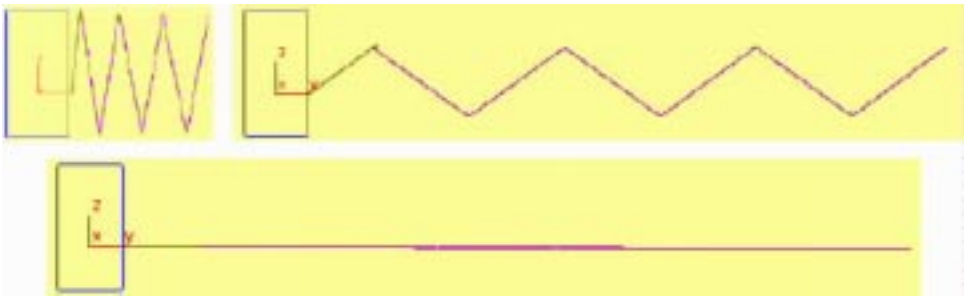

Figure 9. Shots of the solar array deployment steps.

In the following four models are used. Noting that all eigenmodes (em) are computed for free-free structures and all frequency response modes (frm) are computed for the true joint and force configurations, the models are in detail:

(1) yoke with 15 em, panels with 8 em (604)

(2) yoke with 19 em, panels with 8 em (690)

(3) yoke with 5 em + 11 frm, panels with 8 em (583)

(4) yoke with 5 em + 11 frm, panels 5 em + 13 frm (1953),

where the brackets give the necessary CPU time in seconds.

According to what was said before participation factors for free-free eigenmodes of the yoke and panels are computed for the static equilibrium phase after the jump out and after complete deployment, since these are the interesting points in time. Figure 10 show the simulation results for the flexible displacements of a marker in the middle of the last panel in x and about y -axis.

Figure 10 shows an increasing deviation of the results for an increasing number of used frm. For the case at hand the simulation results are basically determined by two very different groups of mode shapes: the first few em are very suitable for representing the biggest part of the energy or, in other words, of the overall deformations. The frm on the other hand were computed letting Ω_0 = 2 Hz in Equation (28), which after making the mass and stiffness matrices orthogonal gave frequencies ranging from 2 to 800 Hz, thus representing mostly high frequency oscillations. As expected, these oscillations represent only small amounts of energy with the main panel plane almost staying at rest while all little appendages and flanges are moving furiously. But it is exactly these points where the above mentioned cable loops are attached. It is therefore believed that modes that represent these special motions of the appendages give results closer to reality than other modes. With these findings the proper strategy of mode selection would be to apply the participation factor method to find say, the four or five most important low frequency eigenmodes for the most interesting force configurations to represent the overall flexible behaviour and to use the frm method to find the high frequency modes that represent motions of interesting physical locations on each flexible structure. Further research on this topic is on the way.

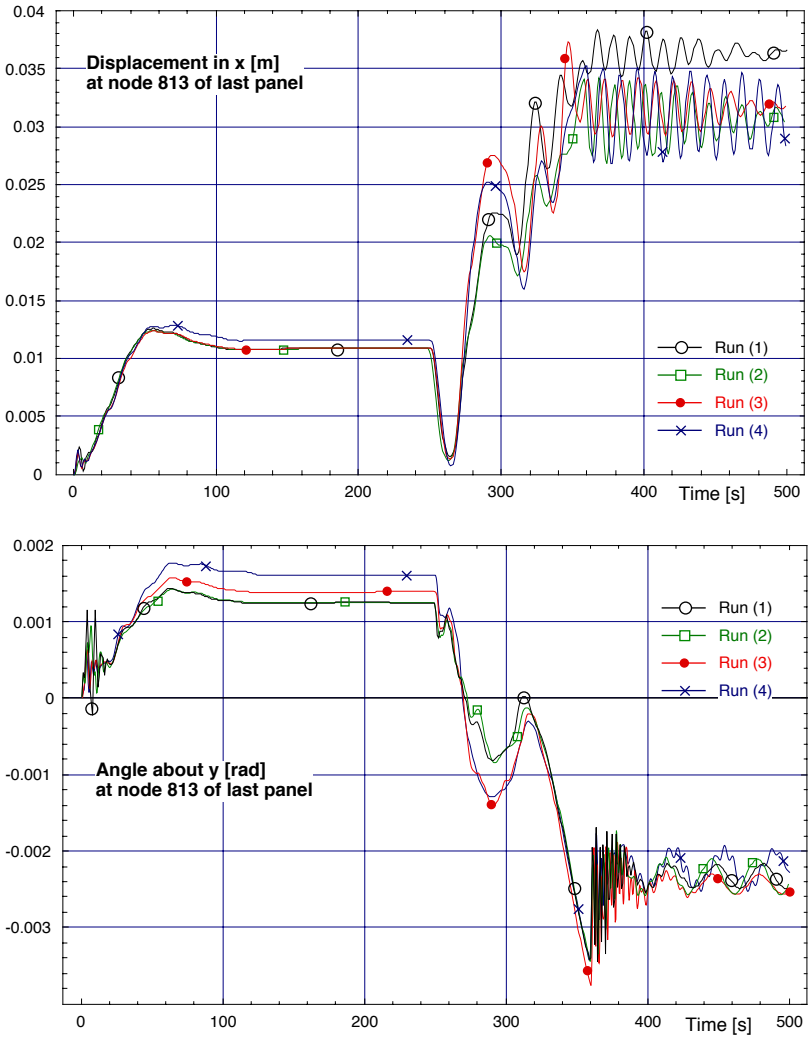

Figure 10. Displacements of the last panel.

5. Conclusion

This paper discusses the influence of a nonlinear formulation of flexible deformations using second order terms and presents methods for a proper selection of mode shapes for dynamical multibody analyses.

It is found that using quadratic terms to describe deformation proves beneficial if large forces are acting on slender structures that show effects of coupled tension, bending and torsion, as is the case for the example stabilisation linkage.

For extended simulations such as the deployment of a solar array in space only a modal representation of deformations is practical, giving rise to the problem of selecting proper modes. Here we propose the use of participation factors to select eigenmodes for representation

of the main deformations and to use frequency response modes to represent high frequency local flexible motions at the spots of interest. An estimation error of the deformations displacements can be found for the reduced mode shape model with respect to a model including all available mode shapes.

References

1. S. Dietz, *Vibration and Fatigue Analysis of Vehicle Systems Using Component Modes*, Berlin, Dissertation, Fortschritt-Berichte VDI, Reihe 12: Verkehrstechnik/Fahrzeugtechnik, Nr. 401, Düsseldorf, VDI-Verlag, 1999.

2. S. v. Dombrowski, *Analysis of Large Flexible Body Deformation in Multibody Systems Using Absolute Coordinates.* Multibody System Dynamics, 8, 2002, pp. 409-432.

3. C. Pösl, *Erweiterung und Testen des Moduls SimBeam uner SIMPACK*, Fachhochschule München, Diplom Thesis, 2002.

4. W. Rulka, A. Eichberger, *SIMPACK: An Analysis and Design Tool for Mechanical Systems,* in *Multibody Computer Codes in Vehicle System Dynamics,* (W. Kortüm and R. S. Sharp, ed.), Vol. 22, Supplement to Vehicle System Dynamics, Swets and Zeitlinger, Amsterdam, 1993, pp. 122-126.

5. R. Schwertassek, O. Wallrapp, *Dynamik flexibler Mehrkörpersysteme*. Friedr. Vieweg Verlag, Braunschweig, 1999.

6. R. Schwertassek, O. Wallrapp, S. v. Dombrowski, *Modal Representation of Stress in Flexible Multibody Simulation.* Nonlinear Dynamics, 20(4), 1999, pp. 381-399.

7. R. Schwertassek, O. Wallrapp, A. Shabana, *Flexible Multibody Simulation and Choice of Shape Functions.* Nonlinear Dynamics, 20(4), 1999, pp. 361-380.

8. A. A. Shabana, *Flexible Multibody Dynamics: Review of Past and Recent Developments.* Multibody System Dynamics, 1, 1997, pp. 189-222.

9. O. Wallrapp, *Standardization of Flexible Body Modeling in Multibody System Codes, Part I: Definition of Standard Input Data.* Mechanics of Structures and Machines, 22(3), 1994, pp. 283-304.

10. O. Wallrapp, *Nonlinear Beam Theory in Flexible Multibody Dynamics - Theory of SIMBEAM*, Intec GmbH, Wessling, Report Version March 2002.

11. O. Wallrapp, R. Schwertassek, *Representation of Geometric Stiffening in Multibody System Simulation.* Int. Journal for Numerical Methods in Engineering, 32, 1991, pp. 1833-1850.

12. O. Wallrapp, S. Wiedemann, *Simulation of Deployment of a Flexible Solar Array.* Multibody System Dynamics, 7, 2002, pp. 101-125.

List of Figure Captions

List of Tables

Table 1. Load cases for simulations of the linkage.

Load Case	Suspension	Forces at node 20	Torques at node 20
1	clamped at node 1	30, 30, 30 N	0, 0, 0 Nm
2	see 1	100, 100, 100 N	0, 0, 0 Nm
3	*x* at node 1 *x, y, z* at node 7 *x, z* at node 14	0, 0, -1000 N	0, 0, 0 Nm
4	see 3	0, 0, 1000 · sin (2 π *t*)	0, 0, 0 Nm

Table 2. Deformation of the linkage for load cases 1, 2 and 3.

For models (A) to (C) the errors are given with respect to ANCF or nonlinear ANSYS results.

Load	Model of	Displacements / Error in % at node 20					
Case	approxim.	$u_x$mm	u_y mm	u_z mm	ϑ_x rad	ϑ_y rad	ϑ_z rad
1	ANCF	16.119	3.3638	14.771	0.01768	0.00745	-0.0231
	(A)	1	9	1	1	1	1
	(B)	-1	8	0	0	1	0
	(C)	0	1	0	0	-1	0
2	ANCF	53.034	9.1563	47.936	0.05726	0.02428	-0.0753
	ANSYS	53.002	9.1400	47.901	0.05731	0.02432	-0.0754
	(A)	2	33	4	4	3	3
	(B)	-2	30	2	2	2	1
	(C)	0	4	1	1	3	1
3	ANSYS	4.9446	-1.3406	-51.328	-0.0466	-0.2123	0.0093
	(A)	-83	-186	44	42	44	-124
	(B)	-100	-178	4	-3	9	-134
	(C)	-31	52	5	-2	8	-74

Table 3. Deformation of the linkage for load cases 2 and 3.

The errors are given with respect to nonlinear ANSYS results.

em = eigenmodes, pf = selected using participation factors, frm = frequency response modes.

Load	Model of	Displacements / Error in % at node 20					
Case	approxim.	$u_x$mm	u_y mm	u_z mm	ϑ_x rad	ϑ_y rad	ϑ_z rad
2	ANSYS	53.034	9.1563	47.936	0.0573	0.02428	-0.0754
	all 114 em	1	2	3	3	13	2
	first 10 em	-27	24	-39	-32	-40	-17
	first 15 em	-22	18	-27	-19	-46	-13
	19 em-pf	-11	13	-16	-13	-9	-10
	3em+12frm	2	2	4	5	-11	2
3	ANSYS	4.9446	-1.3406	-51.328	-0.0466	-0.2123	0.0093
	all 114 em	-9	-57	0	0	4	-89
	14 em-pf	-9	-54	0	2	3	-83
	3em+12frm	-9	-57	0	0	4	-89